



## EFFECTS OF AIR BLOWING ON TURBULENT FLOW OVER A CIRCULAR CYLINDER

Buryan APACOGLU, Akin PAKSOY and Selin ARADAG\*

TOBB University of Economics and Technology, Department of Mechanical Engineering  
Sogutozu Cad. No: 43, 06560, Ankara, \*saradag@etu.edu.tr

(Geliş Tarihi: 05. 10. 2010, Kabul Tarihi: 28. 03. 2011)

**Abstract:** This study analyzes the flow over a two-dimensional (2D) circular cylinder at a turbulent Reynolds number of 20,000 and its control by air blowing from several slots located on the surface of the cylinder, computationally. CFD simulations are performed by using Unsteady Reynolds-Averaged Navier-Stokes (URANS) equations and Spalart-Allmaras turbulence model. Uncontrolled flow simulation results are validated using the experimental results available in literature for drag coefficient, Strouhal number, time-averaged pressure coefficient distribution on the circumference of the cylinder and mean velocity values at the downstream. Air blowing from several slots located on the cylinder is used as an actuator for forcing the flow. Blowing from four slots located on the circumference of the cylinder with a velocity magnitude of 50% of the free stream velocity yields a drag reduction of 23% compared to the uncontrolled case. Additionally, near wake region is further examined by application of Proper Orthogonal Decomposition (POD) technique. A Fast Fourier Transform (FFT) based spatial filtering procedure is employed in order to separate the effects of small-scale turbulent structures in the wake region. The FFT-filtered snapshot-based POD analysis shows that approximately 99% of the total energy of the flow can be represented by considering only the most energetic first two modes where the effects of von Karman vortex street can be seen appropriately both for uncontrolled and controlled flow cases.

**Keywords:** Circular cylinder, Von Karman vortex street, Flow control, Blowing, Proper Orthogonal Decomposition.

## HAVA ÜFLEMENİN DAİRESEL SİLİNDİR ÜZERİNDEKİ TÜRBÜLANSLI AKIŞA ETKİLERİ

**Özet:** Bu çalışmada, Reynolds sayısı 20,000 iken iki-boyutlu (2B) silindir üzerindeki türbülanslı akış ve silindir üzerine yerleştirilen deliklerden hava üfleme ile bu akışın kontrolü sayısal olarak incelenmektedir. Hesaplamalı Akışkanlar Dinamiği (HAD) benzetimlerinde Zamana-bağlı Reynolds-Ortalamalı Navier-Stokes (URANS) denklemleri ve Spalart-Allmaras türbülans modeli kullanılmıştır. Kontrolsüz akış benzetimleri literatürde yer alan sürüklenme katsayısı, Strouhal sayısı, silindir üzerindeki ortalama basınç katsayısı dağılımı ve silindir arkası alandaki ortalama hız dağılımı ile doğrulanmıştır. Silindirin üzerine yerleştirilen deliklerden hava üflemenin eyleyici olarak kullanılmasıyla akış kontrolü gerçekleştirilmiştir. Silindirin yüzeyine yerleştirilen dört adet delikten akış hızının %50'si büyüklüğünde bir hızla hava üflenmesi ile kontrolsüz duruma kıyasla sürüklenme katsayısında %23 azalma görülmüştür. Ayrıca, silindirin arkasındaki yakın alan, HAD analizleri sonucunda elde edilen veri topluluğuna Dikgen Ayırıştırma Yöntemi (DAY) uygulanması ile detaylı olarak incelenmiştir. 2B akışa Hızlı Fourier Dönüşümü (HFD) filtrelemeli olarak anlık durum-tabanlı DAY uygulanmasıyla kontrolsüz ve kontrollü akışlar için akışın toplam enerjisinin %99'u yalnızca en yüksek enerjiye sahip iki kip ile gösterilmiştir. Bu kiplerde von Karman girdap yolu düzgün bir biçimde görülmektedir.

**Anahtar Kelimeler:** Dairesel silindir, Von Karman girdap yolu, Akış kontrolü, Üfleme, Dikgen Ayırıştırma Yöntemi.

### NOMENCLATURE

$C$	Covariance matrix	$u$	Blowing velocity
$C_D$	Drag coefficient [ $F_D/(0.5\rho U^2 A)$ ]	$U$	Free-stream velocity
$C_p$	Pressure coefficient [ $C_p=(P-P_\infty)/(0.5\rho U^2)$ ]	$\bar{U}$	Mean of the CFD data ensemble
$D$	Diameter of the cylinder [m]	$\alpha_{ik}$	Time dependent coefficient defined for the $k^{th}$ mode and $i^{th}$ snapshot
$ds$	First cell height [m]	$\Delta t$	Time step
$M$	Number of total snapshots	$\Delta x$	Spatial increment in the x-direction
$Re$	Reynolds number [ $\rho U D/\mu$ ]	$\Delta y$	Spatial increment in the y-direction
$S$	Necessary mode number	$\phi_k(\mathbf{x})$	$k^{th}$ basis function representing the $k^{th}$ mode
$St$	Strouhal number [ $fD/U$ ]		

## INTRODUCTION

Flow over bluff bodies is an important research area due to its wide range of engineering applications. Although, the geometry of a bluff body can be simple, the flow behind it is chaotic and time-dependent after a certain value of Reynolds number. Forces acting on the body also vary in time, and can cause periodic loading on the body. These forces originate from momentum transfer from fluid to the body, and they are strongly related to the shape of the body and properties of the flow.

Flow over a circular cylinder problem arises in diverse engineering applications such as hydrodynamic loading on marine pipelines, risers, offshore platform support legs, chemical mixing, lift enhancement etc. (Ong *et al.*, 2009; Gillies, 1998). It is experimentally investigated by Norberg (1987) that when the Reynolds number (Re) of flow over a circular cylinder exceeds 48, vortices separate from the boundary layer, and start to move through the downstream, where steady state behavior of the flow turns into a time-dependent state. These periodically moving vortices through the downstream form self-excited oscillations called the von Karman vortex street.

Separation from the surface of the cylinder can be either laminar or turbulent according to the regime of the flow in the boundary layer. Flow with a Reynolds number between 1,000 and 200,000 is called subcritical, and in this range, boundary layer on the cylinder is entirely laminar, and transition from laminar to turbulent flow happens somewhere at the downstream (Wissink and Rodi, 2008). Up to  $Re=100,000$ , flow is characterized by purely laminar separation at  $80^\circ$  from the first stagnation point (Kwok, 1986).

Several experimental and computational studies in literature examine the flow over a circular cylinder at subcritical Reynolds numbers. For  $Re=20,000$  experimental data provided by Anderson (1991), Aradag *et al.* (2009), and Lim and Lee (2002) show that drag coefficient ( $C_D$ ) for flow over a circular cylinder is between 1.16 and 1.2. Schlichting and Gersten (2003) state that Strouhal number (St) is 0.21 at the same flow conditions. Also, the flow over a three-dimensional (3D) circular cylinder is analyzed by Aradag (2009) using Large Eddy Simulation (LES) without a subgrid turbulence modeling, where  $C_D$  and St number are evaluated as 1.2 and 0.2 respectively.

There are several engineering applications that are concerned with the control of the vortices formed behind the cylinder such as vibration control, chemical mixing improvement, dynamic stall control and lift enhancement. Different active control schemes are utilized in literature for damping the vortex-induced oscillations, such as acoustic excitation, rotation of the cylinder, alternate blowing and suction at separation points, and vibration wires in the wake (Gillies, 1998).

The dynamical and thermal behavior of the flow around a circular cylinder submitted to blowing is experimentally investigated by Mathelin *et al.* (2005).

In this study, blowing is applied continuously from the surface of a porous cylinder at Reynolds numbers ranging from 3,900 to 14,000. Different injection rates are tested, and it is observed that the boundary layer thickness (BLT) increases dramatically with increasing injection rates (BLT is doubled under an injection rate of 5%). This results in a lower friction stress and a decrease in the viscous drag of the cylinder due to lower normal velocity gradient obtained under blowing. This can be used as an actuator to control the vortices shedding from the cylinder and to reduce the drag force acting on the cylinder.

Blowing from discrete locations on the surface of the cylinder is examined by Zhdanov *et al.* (2001) at a Reynolds number of 15,000 computationally. In this study, slots with a length of 0.1 D are located at the trailing side of the cylinder and blowing is activated with a velocity of 65% of the free stream velocity. As a result of this numerical experiment, slight decrease in drag coefficient is observed. When the results of the studies performed by Mathelin *et al.* (2005) and Zhdanov *et al.* (2001) are compared, it is clear that the locations of the blowing slots play a crucial role on flow distribution and drag reduction.

There are different classification schemes for flow control methods. General classification scheme for flow control methods considers energy expenditure and involves the control loop. A passive control device does not require any auxiliary power and control loop, on the other hand, active control requires energy expenditure. (Gad-el-Hak, 2000). Blowing is an active flow control technique and requires energy expenditure. Therefore, velocity of the blown air and dimension of the slot, which are the parameters that affect mass flow rate, become important factors that can make the control strategy more or less effective.

In closed loop control, process variable is measured, compared to a set point and an action is taken to correct any deviation from the set point. On the other hand, in open loop control there is no comparison between process variable and set point. It is regardless to the process variable conditions after control actuator takes action; therefore, output variable does not have any influence on the input variable (Process Control System, 2010). Before developing a closed loop control strategy, it is a priority to determine the effect of the actuator (blown air) on the system (flow around the cylinder). This study analyzes the effect of blowing and, because of this reason; the control loop is open, and no sensors are required.

The Proper Orthogonal Decomposition (POD) is a reduced order modeling technique used to analyze experimental and computational data by identifying the most energetic modes in a sequence of snapshots from a time-dependent system (Cao *et al.*, 2006). It was used in numerous applications to introduce low-dimensional descriptions of system dynamics by extracting dominant features and trends (Lumley, 1967). The POD technique was originally introduced by Karhunen and Loève,

which has several distinct names among different disciplines as Karhunen-Loève Decomposition, Principal Component Analysis and Singular Systems Analysis (Holmes *et al.*, 1996). The major theory of the POD technique offers infinite linear combinations of orthogonal functions to represent a stochastic process or a system (Newman, 1996).

The POD technique was developed in the context of pattern recognition, and it has been used successfully as a method for determining a low-dimensional description for human face, structural vibrations, damage detection and turbulent fluid flows (Chatterjee, 2000). In addition, the method has also been used for industrial and natural applications, such as supersonic jet modeling, thermal processing of foods, investigation of the dynamic wind pressures acting on buildings, weather forecasting and operational oceanography (Cao *et al.*, 2006).

Among a variety of fluid-based application areas, in a case explored by O'Donnell and Helenbrook (2007), the POD technique is used to capture the parametric variation of a flow with Reynolds number by reducing the degrees of freedom needed to solve a system of partial differential equations numerically to describe the fundamental physics of particle flows. The authors studied incompressible, axisymmetric, steady flow over spherical particles at various Reynolds numbers in order to give alternative correlation approaches for predicting drag on a sphere. In another case studied by Sen *et al.* (2007), the technique is used as a tool to obtain a clear understanding of the nature of the effect of surface roughness. In the research, a rough-wall turbulent boundary layer in a channel, where a velocity database obtained by Direct Numerical Simulation (DNS), is used to extract the dominant features and trends in the flow by application of the POD technique. In an interesting research performed by Connell and Kulasiri (2005), POD is based on analyzing the turbulent structures of water flow using the Navier-Stokes equations for floods of rivers. In this research, the authors studied the POD technique to decompose the velocity vectors into modes that exist for each direction from the data collected by Particle Image Velocimetry (PIV) measurements. Their scope includes developing a model for turbulent fluctuations and waves formed in rivers based on Navier-Stokes equations by using the POD modes simulating the turbulent structures (Connell and Kulasiri, 2005). Another research that shows the potential of the POD technique is performed by Lieu *et al.* (2006). In this study, the authors stated that the POD method can be used to obtain reduced-order aeroelastic modeling of a complete F-16 fighter aircraft configuration in the transonic regime for possible future real time analyses (Lieu *et al.*, 2006).

The flow in fluid mechanics systems that have turbulence is complex and flow structures display different ranges of length scales. In energetic and randomly characterized turbulent flows, direct application of the snapshot-based POD approach (Sirovich, 1987) to the CFD data ensemble poses

problems (Ma and Karniadakis, 2002). Hence, in order to observe the wake region effectively, utilization of a filtering procedure is essential to eliminate the effects of small-scale turbulent fluctuations, and the remaining unwanted bifurcations. In addition, only considering large-scale eddies and their representations by POD modes is sufficient to control the flow, since energy is transferred from large eddies to the smaller ones, sequentially (Frisch, 1995).

This research contains a series of computational studies that analyze turbulent flow over a two-dimensional circular cylinder with laminar separation at a Reynolds number of 20,000 and its open loop control by air-blowing from slots located on the surface of the cylinder. Additionally, POD technique combined with spatial Fast Fourier Transform (FFT) filtering procedure proposed by Aradag *et al.* (2010) is used as a post-processing tool to reduce the order of the flow and to observe the effects of dominant large-scale turbulent structures in the wake region.

## METHODOLOGY

The method of research involves CFD analyses, validation of the simulations performed using the experimental results in literature, control of the flow by air blowing from the surface of the cylinder and implementation of the FFT-filtered snapshot-based POD technique for reduced order modeling of the flow to further analyze flow dynamics.

### CFD Methodology

CFD simulations are performed by using URANS equations and Spalart-Allmaras turbulence modeling. Incompressible turbulent flow is modeled with double precision in the simulations. Conservation of mass (Eq.1) and momentum (Eq. 2) equations solved are as follows:

$$\rho \frac{\partial u_i}{\partial x_i} = 0 \quad (1)$$

$$\rho \left[ \frac{\partial u_i}{\partial t} + \frac{\partial (u_i u_j)}{\partial x_j} \right] = -\frac{\partial p}{\partial x_i} + \frac{\partial}{\partial x_j} \left[ \mu \left( \frac{\partial u_i}{\partial x_j} + \frac{\partial u_j}{\partial x_i} \right) \right] + \frac{\partial (-\rho \overline{u'_i u'_j})}{\partial x_j} \quad (2)$$

Boussinesq approximation given by Eq. (3) is utilized to model Reynolds stress ( $-\rho \overline{u'_i u'_j}$ ) term in Eq. (2):

$$-\rho \overline{u'_i u'_j} = \mu_t \left( \frac{\partial u_i}{\partial x_j} + \frac{\partial u_j}{\partial x_i} \right) \quad (3)$$

Eq. (1), Eq. (2) and Eq. (3) are solved computationally by using ANSYS Fluent (v12) software. Detailed information about the Spalart-Almaras turbulence modeling can be retrieved from the original study of Spalart and Almaras (1992). Default constants for turbulence modeling in the software are used in the simulations (ANSYS Fluent Theory Guide, 2009).

Numerical methods and solution algorithms employed in CFD simulations are as follows:

- Coupled algorithm for pressure-velocity coupling
- Second-order upwind method for spatial discretization
- First-order temporal discretization
- Least squares cell-based method for calculations of gradients and derivatives

Operating conditions and fluid properties are selected as density= $0.01056 \text{ kg.m}^{-3}$ , velocity= $34 \text{ m.s}^{-1}$ , viscosity= $1.795 \times 10^{-5} \text{ kg.(m.s)}^{-1}$  and pressure= $872.36 \text{ Pa}$ . Free-stream velocity is defined at the inlet boundary with a turbulence intensity of 10% and a length scale of 0.07 m. High turbulence intensity is used as an initial perturbation to trigger unsteadiness of the vortex shedding from the surface of the cylinder instead of defining an angle of attack at the inlet (Aradag *et al.*, 2010). Outlet-vent boundary condition is applied at the outlet, and top and bottom surfaces are defined as symmetrical. Surface of the cylinder is defined as smooth wall, and no-slip boundary condition is employed.

The dimensions of the computational domain are defined as 40 m x 40 m and the cylinder, diameter of which is equal to 1 m, is placed at the center of this domain (Fig. 1).

The grid is generated by using quadrilateral elements around the surface of the cylinder, and triangular cells at the other parts of the computational domain. The grid behind the cylinder is tightened to obtain a finer grid, and to reduce the numerical errors at the downstream.

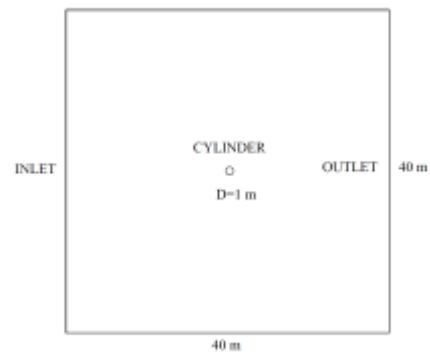
To obtain an accurate boundary layer solution, adequate amount of nodes should be implemented in the boundary layer. Non-dimensional wall distance ( $y^+$ ) is a dimensionless number that gives information about the distance of the cell from the wall.  $y^+ < 5$  corresponds to viscous sublayer in which momentum is transferred from flow to the body by only molecular processes (Kakac and Yener, 1994). To resolve boundary layer accurately, several numbers of nodes should be implemented in viscous sublayer region. Although  $y^+ = 1$  (5 nodes) can fully resolve the viscous sublayer (Unal and Goren, 2011), it is proposed to generate grids with a  $y^+$  value smaller than 0.2 (that corresponds to 25 nodes) to obtain a solution with higher accuracy. According to NASA viscous grid spacing calculator<sup>1</sup>, first cell height ( $ds$ ) is computed as 0.1545 mm for  $D=1 \text{ m}$  and  $y^+ = 0.2$  at  $Re=20,000$ . With this information, the first cell height ( $ds$ ) is selected as 0.15 mm and 0.10 mm respectively for the first and second grid structures (Fig. 2). For both grids  $y^+$  value is smaller than 0.2. Detailed information of the generated grids is given in Table 1.

Table 2 shows drag coefficients ( $C_D$ ) and Strouhal number ( $St$ ) values for simulations performed with two different grids. Spalart-Allmaras turbulence model is used to model turbulent structures since it is very

efficient for external air flows with separations (ANYS Fluent Theory Guide, 2009).

For  $Re=20,000$ , experimental values of  $C_D$  found in literature is between 1.16 and 1.2, while  $St$  is 0.21. Computed  $C_D$  and  $St$  values are close to the experimental ones for the computations with both of the grids. However, resultant  $C_D$  value of the first grid is in the range of experimental values, and it yields a  $St$  value with a smaller difference compared to the experimental one. Therefore, Grid-1 is selected for further analyses. It contains four slots located on the circumference of the cylinder that enable air blowing from several positions from the surface of the cylinder.

Two different time-step sizes ( $\Delta t$ ) are tested and a vortex shedding period is modeled by approximately 150 and 300 time steps with  $\Delta t = 1 \times 10^{-3}$  seconds and  $\Delta t = 0.5 \times 10^{-3}$  seconds, respectively. Table 3 shows drag coefficients ( $C_D$ ) and Strouhal number ( $St$ ) values obtained as a result of performed simulations with Grid-1. A time step of  $\Delta t = 1 \times 10^{-3}$  seconds is selected for the rest of the calculations.



**Figure 1.** Schematic representation of the computational domain

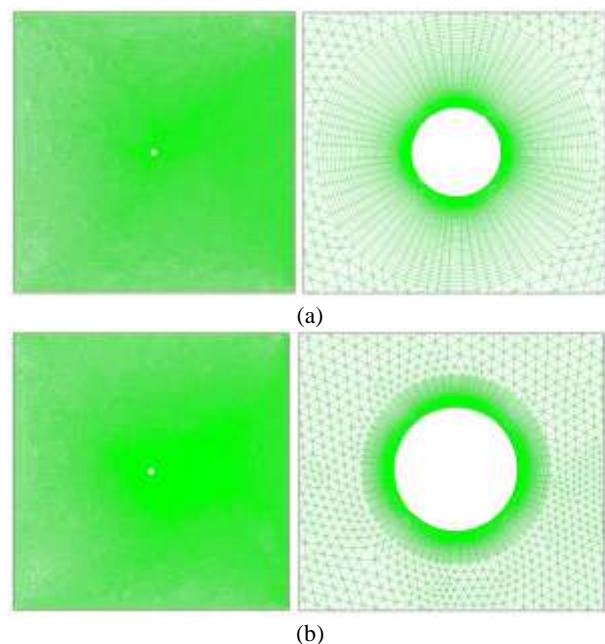


**Figure 2.** Generated grids and their zoom-in near the surface views a) Grid-1 b) Grid-2.

**Table 1.** Grid information.

Grid	Cells	Faces	Nodes
1	72178	112649	40471
2	87668	135204	47554

<sup>†</sup> Retrieved from web site of NASA: <http://geolab.larc.nasa.gov/APPS/YPlus>

**Table 2.** CFD results obtained for analyses performed by Grid-1 and Grid-2, Re=20,000.

Grid	Turbulence Model	C <sub>D</sub>	St
1	S-A <sup>a</sup>	1.17	0.22
2	S-A <sup>a</sup>	1.15	0.23

<sup>a</sup>Spalart-Allmaras (Low-Re Damping)

**Table 3.** CFD results performed by Grid-1 with different time steps.

$\Delta t \times 10^{-3}$ (sec.)	Turbulence Model	C <sub>D</sub>	% diff. <sup>b</sup> for C <sub>D</sub>	St	% diff. <sup>b</sup> for St
1	S-A <sup>a</sup>	1.17	2.5	0.22	4.7
0.5	S-A <sup>a</sup>	1.20	0	0.23	9.5

<sup>a</sup>Spalart-Allmaras (Low-Re Damping)

<sup>b</sup> Abbreviation for *difference*

For controlled flow simulations, air blowing is activated by opening slots located on the surface of the cylinder after 5 seconds of the flow time to avoid initial computational transients. Slots are opened in different combinations and blowing velocities to analyze several control cases. Active control is employed during 5 seconds and approximately 30 vortex shedding periods are observed.

x-velocity values at the wake region are recorded in each time step during 10 periods of flow time in order to obtain data ensemble required for POD application.

### Reduced Order Modeling – Filtering and POD Methodology

In turbulent fluid flows, firstly, large-scale turbulent structures and then by further separation of them through downstream, small-scale turbulent structures are generated in the wake region behind the 2D circular cylinder. The classical snapshot-based POD approach is not able to separate the structures according to their scales. Therefore, a filtering procedure should be performed to experimental or computational turbulent flow data ensemble to observe only the effects of large-scale turbulent structures in the flow field.

There are a couple of filtering methods employed in literature. Examples are given in the studies of Smith *et al.* (2005), Aubry *et al.* (1988), Johansson *et al.* (2002), Gamard and George (2002), and Prazenica *et al.* (2007). In a study performed by Dowell and Hall (2001), the authors used reduced order modeling for fluid-structure interaction. They used temporal pre-filtering to appoint

periodicity, and removed small and stochastic spatial structures. A couple of studies performed by Gamard and George (2002), Attar *et al.* (2006), and Tadmor *et al.* (2008) used a pre-filtering technique to separate small spatial structures in their research.

In this study, filtering the effects of small-scale turbulent structures from the flow field is achieved by application of a Fast Fourier Transform (FFT) method to the data ensemble obtained from CFD analysis. This procedure (FFT-Filtered POD) was originally developed by Aradag *et al.* (2010). After filtering of the data ensemble obtained from CFD simulations, the modified new data ensemble contains only the effects of large-scale turbulent structures, and becomes appropriate for the snapshot-based POD analysis.

The snapshot-based POD method provides a basis for the modal decomposition of an ensemble of functions, containing the data obtained from experiments or computational simulations. The technique was used to analyze data with a view of extracting dominant features and trends named as coherent structures that are typically patterns of space and time (Berkooz *et al.*, 1996). Detailed mathematical procedure for the snapshot-based POD technique is given in Apacoglu *et al.* (2011) and Cohen *et al.* (2006).

## RESULTS

### Baseline Case CFD Results – Uncontrolled Flow Simulations

Drag coefficient (C<sub>D</sub>) and lift coefficient (C<sub>L</sub>) values are monitored during CFD computations and time histories of C<sub>D</sub> and C<sub>L</sub> are obtained. Periodicity in C<sub>D</sub>-history and C<sub>L</sub>-history graphs shown respectively in Fig. 3 and Fig. 4 indicate the periodic behavior of vortex separation from the surface of the cylinder and its effect on drag and lift forces acting on the cylinder. C<sub>D</sub> and C<sub>L</sub> are computed by:

$$C_D = \frac{F_D}{\frac{1}{2} \rho U^2 A} \quad (4)$$

$$C_L = \frac{F_L}{\frac{1}{2} \rho U^2 A} \quad (5)$$

It is clearly seen on C<sub>D</sub> and C<sub>L</sub> histories that flow reaches a periodic state 2 seconds (approximately 15 vortex shedding periods) after the initialization. Solution is free of initial computational transients between 6<sup>th</sup> and 10<sup>th</sup> seconds of the flow time. Therefore, time-averaged values are computed within this time interval. Mean C<sub>D</sub> is calculated within 20 periods of vortex shedding between 6.7 and 9.38 seconds and found as 1.17 which is in the range of experimental values reported in literature (Anderson, 1991, Aradag, 2009, Aradag *et al.*, 2009, and Lim and Lee, 2002).

Pressure distribution on the surface of the cylinder is not uniform because of the circular shape of the cylinder. Pressure acting on the cylinder has an angular dependency and it also changes with time according to vortex shedding from the surface of the cylinder. Time-averaged pressure coefficient ( $C_p$ ) distributions around the circumference of the cylinder versus the angle starting from the stagnation point through the clockwise direction are plotted in Fig. 5. Time-averaged values are computed for 20 periods of vortex shedding between 50<sup>th</sup> and 70<sup>th</sup> periods that are free of initial transients. As seen in Fig. 5, the  $C_p$  distributions are in good agreement with the experimental study performed by Aradag et al (2009) and the computational study performed by Lim and Lee (2002). Eq. (6) is utilized to compute  $C_p$ .

$$C_p = \frac{P - P_\infty}{\frac{1}{2}\rho U^2} \quad (6)$$

Velocity field behind the cylinder is validated with the experimental study of Aradag *et al.* (2009) by comparison of the non-dimensional mean velocity profile, which is at three diameters away from the center of the cylinder at the downstream (Fig. 6). Considering Fig. 6, it is seen that the computed non-dimensional mean velocity profile from the CFD simulations is compatible with the experimental mean velocity profile studied by Aradag *et al.* (2009) and the computational study performed by Aradag (2009).

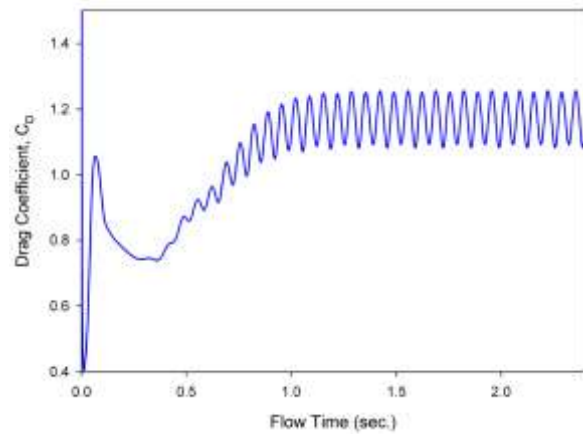


Figure 3. Time history of drag coefficient.

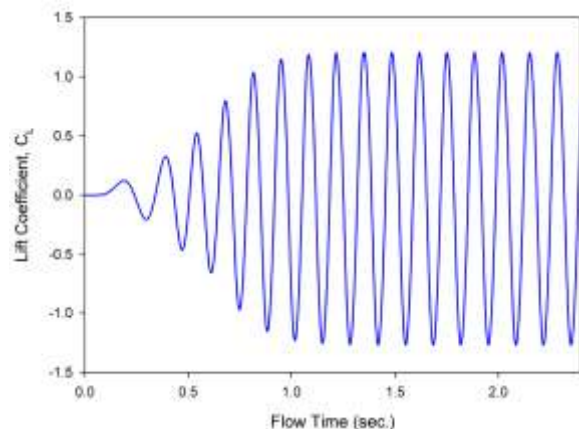


Figure 4. Time history of lift coefficient.

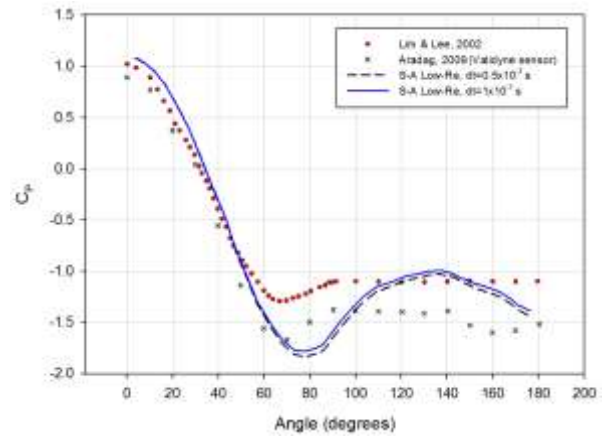


Figure 5.  $C_p$  distributions obtained from CFD simulations and their comparison with the experimental values stated in literature at  $Re=20,000$ .

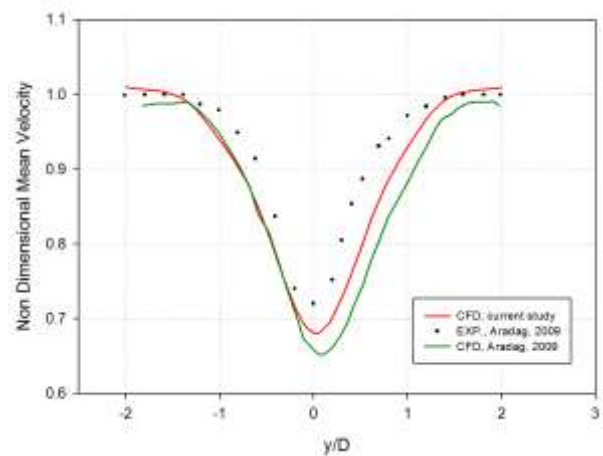


Figure 6. Experimental and computational non-dimensional mean velocity profiles behind the cylinder,  $x=3D$ .

Strouhal number ( $St$ ) is the dimensionless representation of the vortex shedding frequency ( $f$ ) of the flow. It is computed to investigate the periodicity of the flow. Relationship between  $f$  and  $St$  is as follows:

$$St = \frac{fD}{U} \quad (7)$$

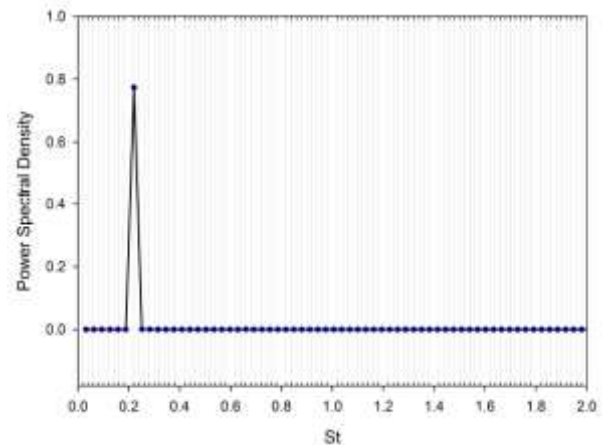
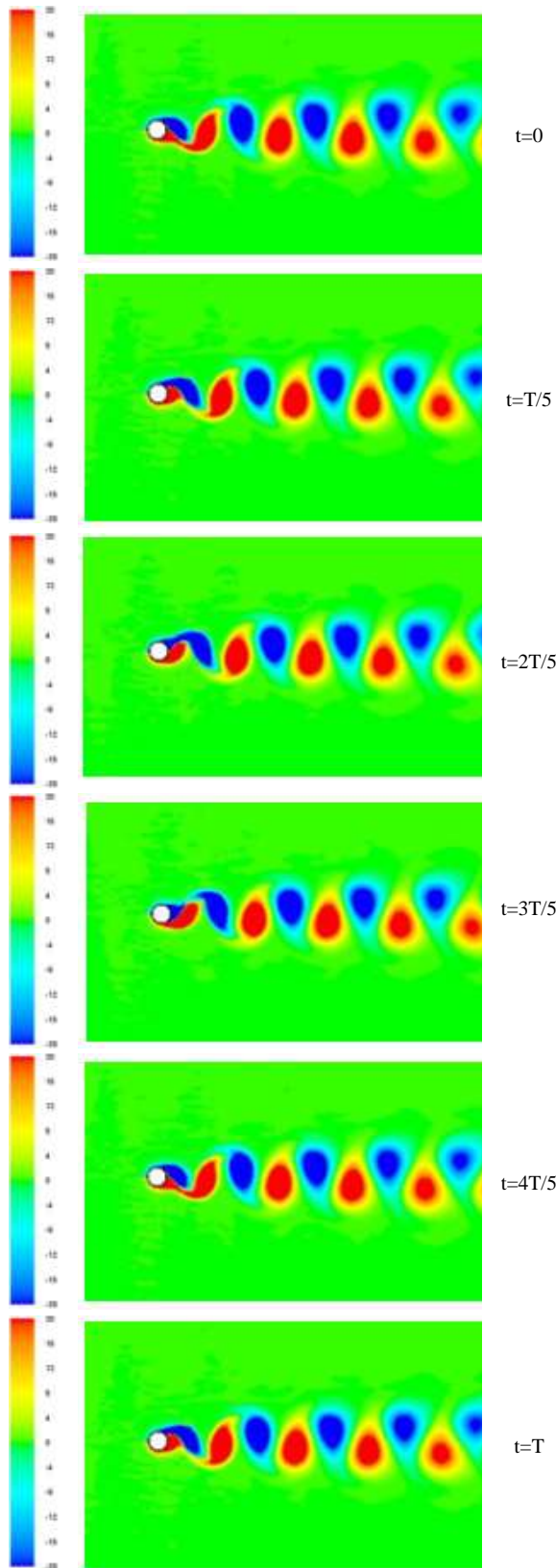


Figure 7. Result of the FFT applied to  $C_L$ -history.

Strouhal number is evaluated by application of Fast Fourier Transform (FFT) to the lift coefficient history (Fig. 7). Peak in Fig. 7 addresses the Strouhal number of the von Karman vortices that are shedding from the surface



**Figure 8.** Contours of Vorticity magnitude at  $t=10$  seconds,  $Re=20,000$ .

and moving through the downstream. Corresponding St number is obtained as 0.22 and therefore, the vortex shedding period (T), which is the reciprocal of vortex shedding frequency, is found as 0.134 seconds. Calculated St number has a 4.7% difference with the experimental one ( $St=0.21$ ) stated by Schlichting and Gersten (2003).

Vorticity contour plots in Fig. 8 show the motion of the fluid during one vortex shedding cycle. The cycle plotted is between 9.000 and 9.134 seconds of the flow time. The von Karman vortex street is clearly seen on vorticity contours. Here, it is important to note that as expected, only large-scale structures, which are the vortices constituting the von Karman vortex street, are resolved accurately by URANS. Hence, it is concluded that the solution performed by URANS can provide adequately accurate data for further POD analysis and flow control applications.

### CFD Results – Controlled Flow Simulations

Totally seven controlled flow cases are examined by opening slots in different combinations with different blowing velocities. The positions of the slots located on the circumference of the cylinder are shown in Fig. 9. The control cases conducted are as follows:

- Blowing from all slots,  $u=0.1 U$
- Blowing from slots numbered 1 and 4,  $u=0.1 U$
- Blowing from slots numbered 1 and 2,  $u=0.1 U$
- Blowing from slots numbered 2 and 3,  $u=0.1 U$
- Blowing from slot numbered 1,  $u=0.1 U$
- Blowing from all slots,  $u=0.5 U$
- Blowing from slots numbered 1 and 4,  $u=0.5 U$

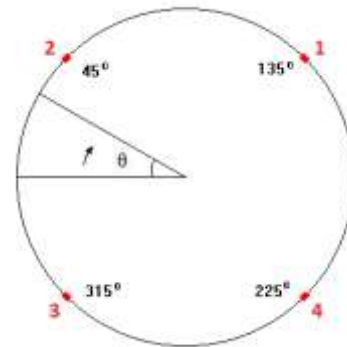


**Figure 9.** Positions of the slots located on the circumference of the cylinder.

Blowing is activated after 5 seconds of the flow time to avoid initial numerical transients. Mean values are calculated within 6-10 seconds time interval that approximately corresponds to 30 vortex shedding periods.  $C_D$  histories with different control cases are given in Fig. 9. Computed mean  $C_D$  values are given in Table 4.

Periodicity of the flow under control is also seen in Fig. 10. There are small changes observed in the vortex

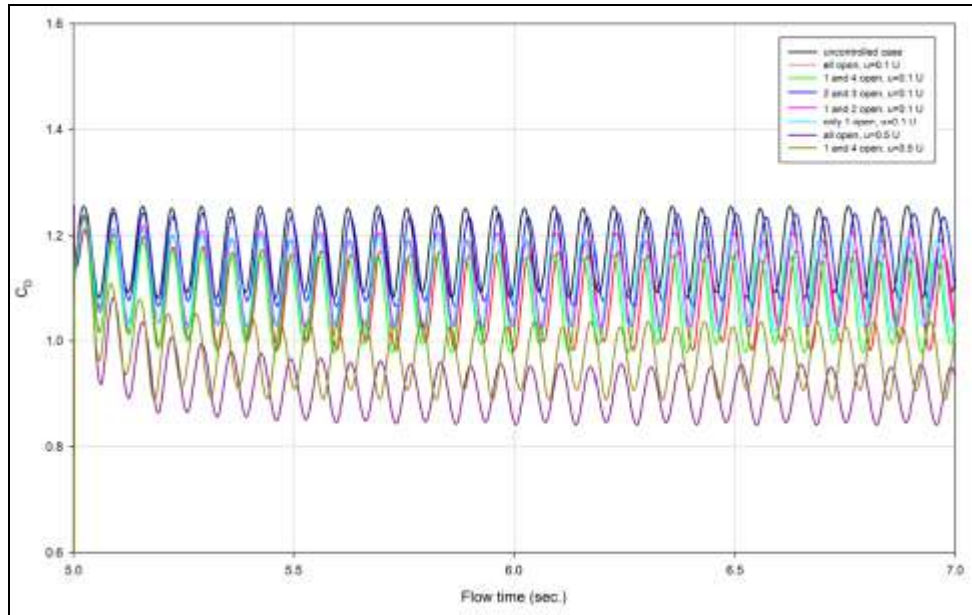


Figure 10.  $C_D$ -histories obtained as a result of uncontrolled and controlled flow cases.

shedding period for controlled flow. To investigate differences between periods further, FFT is applied to  $C_L$ -histories within different time intervals (Table 5). The results of FFT show that changes in periodicity occur temporarily just after the initiation of air blowing. After a while, all control cases converge to the same frequency. Temporary change only causes a phase shift in vortex shedding period.

FFT applied to  $C_L$ -histories between 8-10 seconds of the flow time yields a same  $St$  number that is 0.223 for all controlled flow cases. Period of the flow becomes 0.132 seconds under forcing. Vortex shedding frequency of controlled flow increases and becomes 1.4% higher than the uncontrolled one. This result shows that air blowing from the surface of the cylinder slightly enforces periodicity of the flow.

Figure 11 shows mean  $C_p$  distribution on the circumference of the cylinder that is calculated between 50<sup>th</sup> and 70<sup>th</sup> periods of the flow. In Fig. 11 angular position is measured from the front stagnation point through clockwise direction for all control cases. There are abrupt changes in  $C_p$  distribution near the blowing slots when blowing velocity is 50% of the free-stream velocity.

### Reduced-Order Modeling – Filtering and POD Results

An FFT filtering procedure is adapted to filter the effects of small-scale turbulent structures existing in the data ensemble obtained from the CFD analysis. Later, application of the snapshot-based POD technique to the filtered data ensemble separates only the remaining effects of large-scale turbulent structures of the flow according to their frequency content. Codes are developed to perform both the filtering procedure and

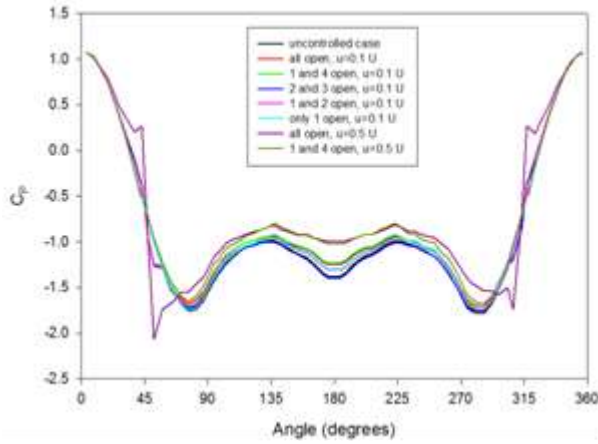
snapshot-based POD application. The details of the FFT-filtering procedure can be found in Aradag et al (2010).

Table 4. Reduction of  $C_D$  by different cases.

$u$	Slots	$C_D$	% reduction
0.1 U	Closed	1.1725	-
	All open	1.0806	7.8
	1 and 4 open	1.0742	8.4
	2 and 3 open	1.1563	1.4
	1 and 2 open	1.1147	4.9
	1 open	1.1103	5.3
0.5 U	All open	0.8992	23.3
	1 and 4 open	0.9656	17.6

Table 5. Results of FFTs applied to  $C_L$ -histories within different time intervals.

$u$	Slots	$St$			
		5-10 sec.	6-10 sec.	7-10 sec.	8-10 sec.
0.1 U	Closed	0.220	0.220	0.220	0.220
	All open	0.220	0.216	0.216	0.223
	1 and 4	0.220	0.223	0.216	0.223
	2 and 3	0.220	0.216	0.216	0.223
	1 and 2	0.220	0.223	0.216	0.223
	1 open	0.220	0.220	0.216	0.223
0.5 U	All open	0.214	0.215	0.216	0.223
	1 and 4	0.233	0.230	0.226	0.223



**Figure 11.**  $C_p$  distribution on the circumference of the cylinder for uncontrolled and controlled flow cases.

In the POD study, the FFT-filtered modified new data ensemble consisting of 1337 and 1320 snapshots respectively for the uncontrolled and controlled flow cases are analyzed. There are totally 10 periods and each period contains 137 and 132 time steps for the uncontrolled and controlled flow analyzes. Snapshots are equally spaced at 0.001 s apart from each other, in which they contain x-velocity data with respect to spatial x and y coordinates.

Table 6 shows the energy content variation with respect to mode number after implementation of the FFT-filtered snapshot-based POD technique to both uncontrolled and the four of the most effective controlled flow cases.

According to Table 6, it is obvious that considering just the first two POD modes reveals approximately 99% of the total energy content for all cases. The energy content for the modes diminishes from mode 1 to mode 4 in all cases. Rate of fall of the energy content is much steeper between the second and third modes.

**Table 6.** Energy contents of the most energetic four POD modes for the uncontrolled, slots 1+4 open and all slots open at  $u=0.1U$  and  $u=0.5U$  controlled cases.

Mode Number	Energy Content (%)				
	Unc. <sup>a</sup>	$u=0.1U$		$u=0.5U$	
		Slots 1+4 Open	All Slots Open	Slots 1+4 Open	All Slots Open
1	54.68	55.31	56.17	55.20	56.96
2	43.96	43.27	42.30	43.77	41.37
3	0.77	0.79	0.85	0.57	0.93
4	0.58	0.63	0.65	0.46	0.72
Total (2 Modes)	98.64	98.58	99.98	98.97	99.98

<sup>a</sup> Abbreviation for *uncontrolled*

Low-dimensional spatial descriptions of the flow field for the most energetic four POD modes related to uncontrolled and two of the most effective controlled flow simulations are shown in Fig. 12. Each POD mode obtained after the snapshot-based POD application onto FFT-filtered data ensemble shows definite characteristics of the flow. The effects of air blowing by different slot combinations with a blowing velocity of  $0.5U$  and vortex formation in the wake region of the 2D circular cylinder can be observed in Fig. 12.

Due to FFT filtering, Fig. 12 shows only the effects of large-scale turbulent structures in the wake region of the 2D circular cylinder. It can clearly be observed from this figure that the formed vortices alternate in time, velocity values changes at certain locations and the effects are dominantly accumulated in the first two modes for the mentioned flow simulation cases.

To provide further analyses on the formed vortices in the flow field, such as a control strategy, observation of the energetic parts of the flow plays a crucial role, and the FFT-filtered POD technique helps to reveal them for the energetic and random turbulent flows.

## CONCLUSIONS

Within the scope of this study, CFD simulations of turbulent flow over a 2D circular cylinder at a Reynolds number of 20,000 are performed and the results are validated using the experimental results in literature. Structure, motion and effects of the von Karman vortices are captured accurately by URANS and Spalart-Allmaras turbulence modeling. Because of this reason, controlled flow simulations are performed further with the same grid and numerical methods. Effects of air blowing from surface of the cylinder are investigated in controlled flow CFD simulations and the flow is further analyzed using the snapshot-based POD.

Air blowing from several discrete locations on the surface of the cylinder is examined in controlled flow simulations by opening the slots in different combinations. 23% drag reduction is achieved by blowing air with a velocity of  $0.5U$  from all the slots on the cylinder surface. This shows that blowing from several discrete locations before and after the separation points is an efficient method for drag reduction purposes. Here, it is important to note that the length of each slot is  $0.01D$ , which corresponds to  $0.01m$  in this study. This shows that small amount of blowing can yield considerable drag reduction by affecting the boundary layer on the cylinder and hence total momentum transfer from the flow to the body.

On the other hand, blowing leads to an increase in vortex shedding frequency by a negligible extent that is 1.4% and abrupt changes in  $C_p$  are observed in the vicinity of the active slots. Because of this sudden change in pressure distribution, some mechanical

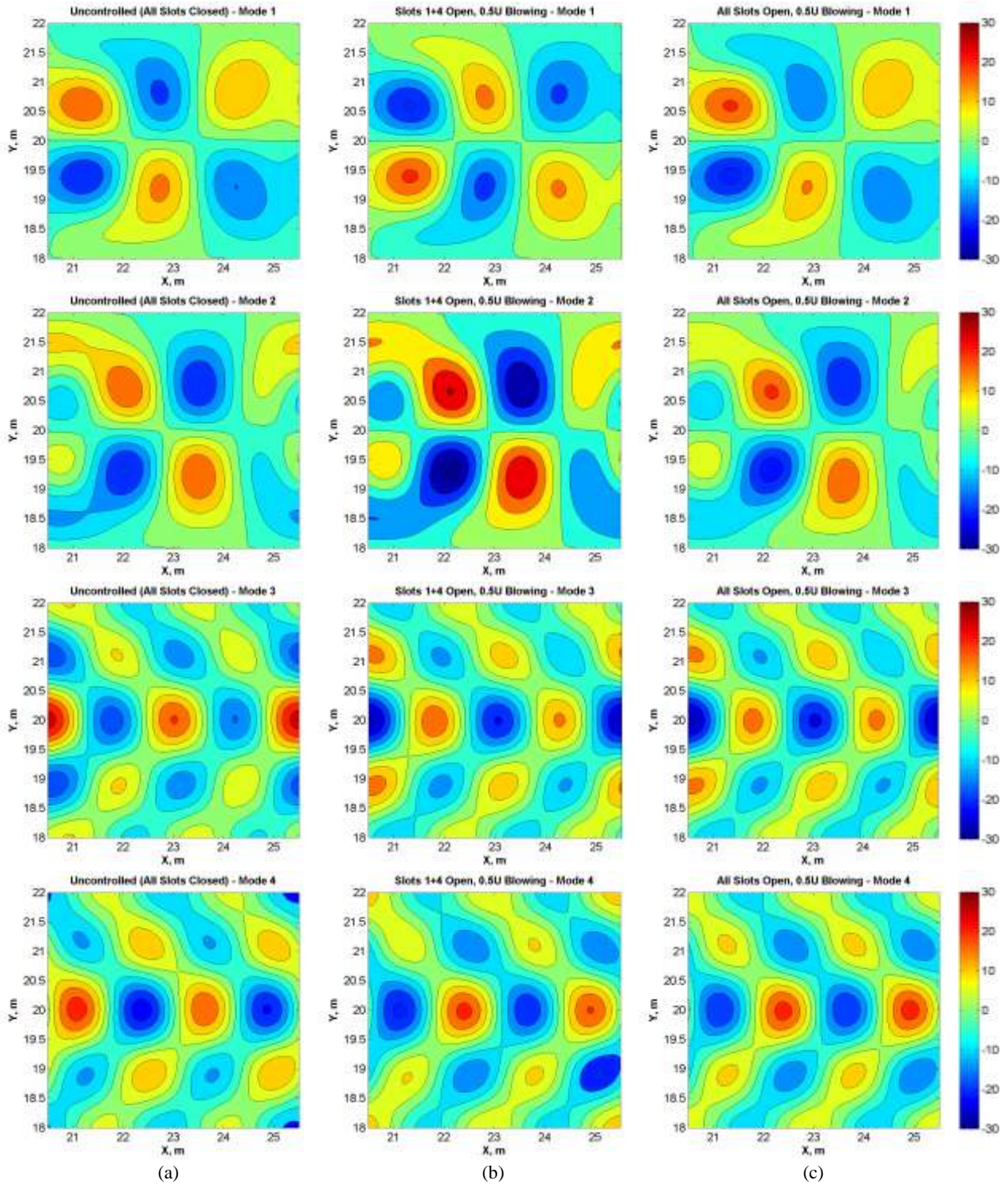


**Figure 12.** The most energetic first four POD modes for a) uncontrolled b) slots 1+4 open 0.5U blowing and c) all slots open 0.5U blowing controlled flow snapshot-based POD analysis

problems may be experienced during flow control such as deformation of the slots, vibration of the cylinder, etc. Therefore, it is suggested to select most convenient control technique according to the engineering application which flow control will be applied.

Since observation of the energetic parts of the flow field, i.e. vortices, is of important for further analyses such as application of a control strategy, FFT filtering integrated snapshot-based POD technique is employed

as a post-processing tool for the CFD data for both controlled and uncontrolled cases. Randomly and energetically characterized turbulent flow fields contain the effects of both large and small-scale turbulent structures; hence, each resulting POD mode contains the effects of these structures at different sizes. Fast Fourier Transform (FFT) based filtering procedure originally developed by Aradag *et al.* (2010) is adapted to observe only the effects of large-scale turbulent structures existing in the wake region of the 2D circular cylinder.

Application of the POD technique reveals that approximately 99% of the total energy of the flow can be represented by using only the most energetic two modes where the formed vortices alternate in time. It is also seen that energy content distribution for the controlled flow does not differ from the uncontrolled one, significantly. Therefore, two of the most energetic POD modes can be utilized in future studies, such as developing a closed loop control strategy.

## ACKNOWLEDGMENTS

This research was supported by The Scientific and Technological Research Council of Turkey (TUBITAK) under grant 108M549. The computations were performed at TOBB University of Economics and Technology CFD Laboratory. The authors would like to thank Dr. Cosku Kasnakoglu for his help related to snapshot-based Proper Orthogonal Decomposition (POD).

## REFERENCES

- Anderson, J. D., *Fundamentals of Aerodynamics*, (Second Ed.), McGraw Hill, New York, 1991.
- ANSYS Fluent v12.0 Software Theory Guide (2009).
- Apacoglu, B., Paksoy A. and Aradag, S., CFD Analysis and Reduced Order Modeling of Uncontrolled and Controlled Laminar Flow over a Circular Cylinder, *Engineering Applications of Computational Fluid Mechanics*, 5(1), 67-82, 2011.
- Aradag, S., Siegel, S., Seidel, J., Cohen, K. and McLaughlin, T., Filtered POD-Based Low-Dimensional Modeling of the Three-Dimensional (3D) Turbulent Flow Behind a Circular Cylinder. *International Journal for Numerical Methods in Fluids*, doi: 10.1002/flid.2238, 2010.
- Aradag, S., Cohen, K., Seaver, C. and McLaughlin, T., Integrating CFD and Experiments for Undergraduate Research, *Computer Applications in Engineering Education*, doi: 10.1002/cae.20278, 2009.
- Aradag, S., Unsteady Vortex Structure behind a Three Dimensional Turbulent Cylinder Wake, *Journal of Thermal Science and Technology* 29(1):91-98, 2009.
- Attar, P. J., Dowell, E. H., White, J. R. and Thomas, J. P., Reduced Order Nonlinear System Identification Methodology, *American Institute of Aeronautics and Astronautics Journal* 44 (8), 1895-1904, 2006.
- Aubry, N., Holmes, P., Lumley, J. and Stone, E., The Dynamics of Coherent Structures in the Wall Region of a Turbulent Boundary Layer, *Journal of Fluid Mechanics* 192, 115-173, 1988.
- Berkooz, G., Holmes, P. and Lumley, J. (1996). *Turbulence, Coherent Structures, Dynamical Systems and Symmetry*, Cambridge University Press, Cambridge, pp. 86-93, 1996.
- Cao, Y., Zhu, J., Luo, Z. and Navon, I., Reduced Order Modeling of the Upper Tropical Pacific Ocean Model Using Proper Orthogonal Decomposition, *Computer and Mathematics with Applications* 52 (8-9), 1373-1386, 2006.
- Chatterjee, A., An Introduction to the Proper Orthogonal Decomposition. *Computational Science Section Tutorial, Department of Engineering Science and Mechanics*, Penn State University, Pennsylvania, USA, 2000.
- Cohen, K., Siegel, S. and McLaughlin T., A Heuristic Approach to Effective Sensor Placement for Modeling of a Cylinder Wake, *Computers and Fluids* 35, 103-120, 2006.
- Connell, R. and Kulasiri, D. Modeling Velocity Structures in Turbulent Flows Using Proper Orthogonal Decomposition, *International Congress on Modeling and Simulation*, December 2005, Melbourne, Australia, 2005.
- Dowell, E. H. and Hall, K. C., Modeling of Fluid Structure Interaction, *Annual Review of Fluid Mechanics* 33, 445-490, doi: 10.1146/annurev.fluid.33.1.445, 2001.
- Frisch, U., *Turbulence: The Legacy of A. N. Kolmogorov*, Cambridge University Press, Cambridge, UK, 1995.
- Gad-el-Hak, M., *Flow Control: Passive, Active and Reactive Flow Management*, Cambridge University Press, 2000.
- Gamard, S. and George, W., Application of a 'Slice' Proper Orthogonal Decomposition to the Far Field of an Axisymmetric Turbulent Jet. *Physics of Fluids* 14(2515), doi: 10.1063/1.1471875, 2002.
- Gillies, E. A., Low Dimensional Control of the Circular Cylinder Wake, *Journal of Fluid Mechanics* 371, 157-178, doi: 10.1017/S0022112098002122, 1998.
- Holmes, P., Lumley, J. L. and Berkooz, G., *Turbulence, Coherent Structures, Dynamical Systems and Symmetry*, Cambridge University Press, Cambridge, UK, 1996.
- Instrumentation and Control: Process Control and Fundamentals (May 2010). See URL. <http://www.scribd.com/doc/25313575/Process-Control-Fundamentals>.
- Johansson, P. B., George, W. and Woodward S. H., Proper Orthogonal Decomposition of an Axisymmetric Turbulent Wake behind a Disk, *Physics of Fluids* 14(2508), doi: 10.1063/1.1476301, 2002.
- Kakac, S. and Yener, Y., *Convective Heat Transfer*, 2<sup>nd</sup> ed., CRC Press, 1994.

- Kwok, K. C. S., Turbulence Effect on Flow Around Circular Cylinder, *Journal of Engineering Mechanics* 112, 1181-1197, 1986.
- Lieu, T., Farhat, C. and Lesoinne, M., Reduced-Order Fluid/Structure Modeling of a Complete Aircraft Configuration, *Computer Methods in Applied Mechanics and Engineering* 195(41-43), 5730-5742, doi: 10.1016/j.cma.2005.08.026, 2006.
- Lim, H., Lee, S., Flow Control of Circular Cylinders with Longitudinal Grooved Surfaces, *American Institute of Aeronautics and Astronautics Journal* 40(10), 2027-2036, 2002.
- Lumley, J. L., The Structure of Inhomogeneous Turbulent Flows, *Atm. Turb. and Wave Prop.*, 1967.
- Ma, X. and Karniadakis, G., A Low-Dimensional Model for Simulating Three-Dimensional Cylinder Flow, *Journal of Fluid Mechanics* 458, 181-190, 2002.
- Mathelin, L., Bataille, F., Lallemand, A., Near Wake of a Circular Cylinder Submitted to Blowing – I Boundary Layers Evolution, *International Journal of Heat and Mass Transfer* 44, 3701-3708, 2005.
- Newman, A. J., Model Reduction via the Karhunen-Loève Expansion Part 2: Some Elementary Examples, Technical Report No. 96-33, *Institute for Systems Research*, 1996.
- Norberg, C., *Effects of Reynolds Number and a Low-Intensity Free Stream Turbulence on the Flow around a Circular Cylinder*, Chalmers University of Technology, ISSN 02809265, 1987.
- O'Donnell, B. J. and Helenbrook, B. T., Proper Orthogonal Decomposition and Incompressible Flow: An Application to Particle Modeling, *Computers and Fluids* 36(7), 1174-1186, 2007.
- Ong, M. C., Utnes, T., Holmedal, L.E., Myrhaug, D., Pettersen, B., Numerical Simulation of Flow around a Smooth Circular Cylinder at very High Reynolds Numbers, *Journal of Marine Structures* 22(2):142-153, 2009.
- Prazenica, R., Kudila, A. J. and Vignola, J. F., Spatial Filtering and Proper Orthogonal Decomposition of Scanning Laser Doppler Vibrometry Data for the Nondestructive Evaluation of Frescoes, *Journal of Sound and Vibration* 304(3-5), 735-751, 2007.
- Process Control System: Control of Temperature, Flow and Filling Level (May 2010). See URL. <http://www.pacontrol.com/download/process-control-systems.pdf>.
- Schlichting, H., Gersten, K., *Boundary Layer Theory*, (Eighth Revised and Enlarged Ed.), Springer, New York, U.S.A., 2003.
- Sen, M., Bhaganagar, K. and Juttijudata, V., Application of Proper Orthogonal Decomposition (POD) to Investigate a Turbulent Boundary Layer in a Channel with Rough Walls, *Journal of Turbulence* 8(41), 2007.
- Sirovich, L., Turbulence and the Dynamics of Coherent Structures, Part I: Coherent Structures, *Quarterly Applied Mathematics* 45(3), 561-571, 1987.
- Smith, T. R., Moehlis, J. and Holmes, P., Low Dimensional Models for Turbulent Plane Couette Flow in a Minimal Flow Unit, *Journal of Fluid Mechanics* 538, 71-110, 2005.
- Spalart, P. R., Allmaras, S. R., A One-Equation Turbulence Model for Aerodynamic Flows, *30<sup>th</sup> Aerospace Sciences Meeting and Exhibit*, AIAA-92-0439, January 6-9, Reno, 1992.
- Tadmor, G., Bisseck, D., Noack, B. R., Morzynsky, M., Colonius, T. and Taira, K. Temporal-Harmonic Specific POD Mode Extraction. *4<sup>th</sup> Flow Control Conference* AIAA paper 2008-4190, Seattle, Washington, USA, 2008.
- Unal, U. O. and Goren, O., Effects of Vortex Generators on the Flow Around a Circular Cylinder: Computational Investigation with Two-Equation Turbulence Models, *Engineering Applications of Computational Fluid Mechanics* 5(1), 99-116, 2011.
- Wissink, J. G. and Rodi, W., Numerical Study of the Near Wake of a Circular Cylinder. *International Journal of Heat and Fluid Flow* 29, 1060-1070, 2008.
- Zhdanov, V. L., Isaev, S. A, Niemann, H. J., Control of the Near Wake of a Circular Cylinder in Blowing Out of Low-Head Jets, *Journal of Engineering Physics and Thermophysics* 74(5), 1100-1103, 2001.



**Buryan APACOGLU**

Buryan Apacoglu was born in Ankara in 1986. She received her BS degree from Hacettepe University, Department of Nuclear Engineering in 2008 and her MS degree from TOBB University of Economics and Technology, Department of Mechanical Engineering in 2010. She was involved in projects funded by The Scientific and Technological Research Council of Turkey and by Ministry of Industry and Trade as a research assistant. Currently, she is working related to nanofluidics for her PhD at TOBB ETU, Department of Mechanical Engineering and works as a teaching assistant at the same university. Her research interests are Computational Fluid Dynamics, Thermal hydraulics and Nanofluidics.



**Akin PAKSOY**

Akin Paksoy was born in Ankara in 1986. He received his BS degree from Hacettepe University, Department of Chemical Engineering in 2009. He is currently continuing his MS degree in TOBB University of Economics and Technology, Department of Mechanical Engineering. At present, he is working in a project granted by The Scientific and Technological Research Council of Turkey as a research assistant. His research focuses on the development of numerical methods with artificial neural networks for flow control systems and reduced order modeling.



**Selin ARADAG**

Dr. Selin Aradag was born in Ankara in 1979. She received her BS and MS degrees from METU, Department of Mechanical Engineering in Ankara in 2000 and 2002. She received her PhD in Mechanical and Aerospace Engineering from Rutgers University in 2006. She worked for the US Air Force Academy for 2 years as a researcher after graduation. Her research interests are in the area of computational fluid dynamics, flow control and high speed flows. Currently, she is an assistant professor at TOBB University of Economics and Technology in Ankara. She is the principal investigator several projects funded by TUBITAK, TUBA, SANTEZ and other institutes.